ARTICLE

Locally Implantable Nanofibre Meshes by Sustained Release of Temozolomide for Combined Thermo-chemotherapy to Treat Glioblastoma

Received 00th January 20xx,
Accepted 00th January 20xx

DOI: 10.1039/x0xx00000x

Emiho Oe[a,b], Nanami Fujisawa[a,b], Lili Chen[a], Koichiro Uto[a], Yoshitaka Matsumoto[c] and Mitsuhiro Ebara*[a,b,d]

Glioblastoma (GBM) is a highly malignant brain tumour that arises from astrocytes or supportive brain tissue in adults. Although there are several therapeutic options, recurrence rates remain high with a 5-year survival rate expectancy of less than 10%. This study investigates nanofibre meshes that allow long-term release of temozolomide (TMZ) over a 4-week period by controlling the fibre morphologies. The nanofibre meshes were fabricated by electrospinning of a biodegradable polymer, poly(*ε*-caprolactone) (PCL). The obtained meshes were flexible and implantable as a local intracranial drug delivery platform. The nanofibre meshes also carry magnetic nanoparticles (MNPs) that enable a combination therapy of hyperthermia/chemotherapy corresponding to alternating magnetic field (AMF). The heat generation behaviour of the nanofibre meshes were successfully adjusted in a hyperthermic temperature range (~42.6°C). The TMZ/MNP-loaded nanofibre meshes showed a 76% reduction in the cell viability of GBM cancer (T98G) cells by the synergistic effect of hyperthermia and chemotherapy. These results indicated their potential applications as implantable intracranial drug delivery systems as an adjunct to surgery and radiation for GBM patients.

1. Introduction

Glioblastoma (GBM) is the most common type of malignant tumour in the central nervous system (CNS), which arises from astrocytes or supportive brain tissue in adults. These tumours show a high proliferation rate and variability in histopathology and diffusely infiltrate adjacent brain tissue, making GBM a very challenging cancer to treat.[1] Conventional therapeutic procedures, aiming to increase patient life expectancy, focus on surgical resection combined with adjuvant radiotherapy and/or orally delivered temozolomide (TMZ) chemotherapy.[2] However, the efficacy of TMZ is very limited, mainly due to the development of resistance, allowing a prolonged survival time of 2 years for 10–27% of patients.[3,4,5] Additionally, haematological toxicity often requires discontinuation of TMZ therapy or prevents dose escalation as dictated by the treatment schedule.[6] Current anti-glioma therapies are not optimally efficient, mainly due to reduced accumulation of TMZ in tumours, systemic toxicity and limited diffusion through the blood–brain barrier (BBB).[7] A number of phase II clinical trials using different alternating scheduling of dose-dense TMZ have shown superior efficacy over the standard TMZ or historical controls with other alkylating agents, including nitrosoureas and procarbazine.[8] Therefore, a need persists for the long-term local sustained release of TMZ, which is expected to reduce side effects by decreasing the systemic circulating dose.

Direct administration into the brain parenchyma of locally implanted drug delivery systems is a powerful strategy and several types of implantable drug delivery devices have been developed.[9] Local delivery also preserves the drug activity and thus potency by avoiding degradation by the liver.[10] Gliadel® wafers were implantable device and composed of biodegradable polymer, which can avoid a second surgery for the implant removal. Gliadel® wafers have been shown to release carmustine over a period of approximately 5 d. However, as much as 80% of carmustine is released within 24 h, and therefore, side effects frequently appear, such as seizures, brain oedema, incomplete wound healing, and intracranial infections.[11,12]

In recent years, nanofibres have attracted much attention as implantable drug delivery platform owing to their large surface area

[a] *Research Center for Functional Materials, National Institute for Materials Science (NIMS), Tsukuba, Japan.*
[b] *Graduate School of Pure and Applied Sciences, University of Tsukuba, Tsukuba, Japan.*
[c] *Department of Radiation Oncology, University of Tsukuba Hospital, Tsukuba, Japan.*
[d] *Graduate School of Advanced Engineering, Department of Materials Science and Technology, Tokyo University of Science, Katsushika-ku, Japan.*
† Footnotes relating to the title and/or authors should appear here.
Electronic Supplementary Information (ESI) available: [details of any supplementary information available should be included here]. See DOI: 10.1039/x0xx00000x

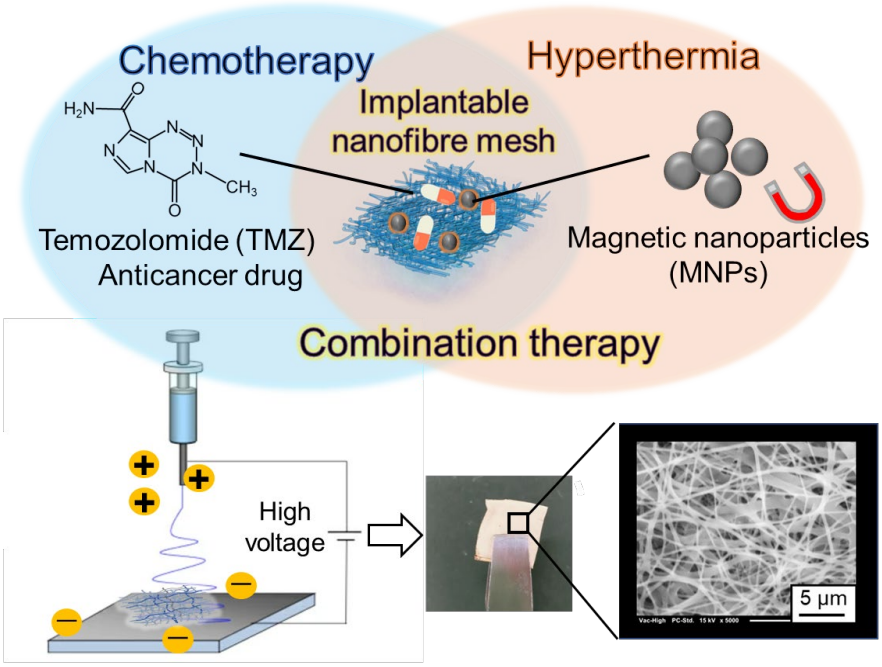

Scheme 1. Schematic illustration of smart nanofibre mesh loaded with MNPs and TMZ to treat GBM. The loaded MNPs generate heat in response to an alternating magnetic field, while the nanofibre allows for the sustained release of TMZ. Both the generated heat and released drug induce cancer cell death by the combination therapy.

and high loading capacity. The use of a nanofibre meshes is a novel alternative method for the local delivery of chemotropic agents to treat GBM.[13–15] Since chemotherapy is often scheduled for 4 weeks, the higher surface area of nanofibres can lead to the longer drug release compared to other drug formulations.[13] Especially, electrospun nanofibres have many advantages compared to other polymer–drug combinational implants because it can achieve higher drug encapsulation efficiency.[16–19] The drug release profiles can be easily designed by controlling the nanofibre diameter.[20,21] Therefore, the optimisation of electrospinning parameters for the control of nanofibres' diameter is significantly important.[22] The electrospinning parameters usually include polymer weight, polymer concentration, solvent type, polymer solution viscosity, and conductivity etc. In addition, process variables need to be considered such as applied voltage, flow rate and tip-collector distance as well as ambient conditions such as temperature and relative humidity.

We have been already developing nanofibre-based local drug delivery platform with different drugs such as methylcobalamin, paclitaxel, doxorubicin, and lenvatinib using biodegradable poly(ε-caprolactone) (PCL)-based electrospun nanofibre meshes.[23–26] We have also successfully incorporated magnetic nanoparticles (MNPs) to generate localized heat which causes heat-induced cell killing as well as enhanced chemotherapeutic effect.[25,26] Hyperthermia is an effective strategy for the treatment of various cancers.[27,28] This strategy is also expected to work for GBM treatment. Therefore, we newly designed nanofibre meshes to achieve a sustained release of TMZ over a 4-week period. The synergistic anticancer effect was also examined upon excitation of the MNP-incorporated meshes with an alternating magnetic field (AMF) (**Scheme 1**). This study presents new insights into an effective locally implantable system for GBM treatment.

2. Materials and Methods

2.1. Materials

PCL (Mw=45k and 80k) (>99.0%), 1,1,1,3,3,3-hexafluoro-2-propanol (HFIP) (>99.0%), and TMZ were purchased from Tokyo Chemical Industry Co., Ltd. (Tokyo, Japan). Iron (III) oxide nanoparticles (MNPs; less than 50 nm particle size) was obtained from Sigma-Aldrich Japan (Tokyo, Japan). Phosphate-buffered saline (PBS) was purchased from Nakalai Tesuque (Kyoto, Japan) (pH 7.4, 0.1% w/v). Roswell Park Memorial Institute (RPMI) 1640 Media was obtained from Thermo Fisher Scientific (Massachusetts, USA). Trypsin, penicillin, and 3-(4,5-dimethylthiazol-2-yl)-2,5-diphenyltetrazolium bromide (MTT) assay reagent were obtained from Nacalai Tesque, Inc. (Kyoto, Japan). Foetal bovine serum (FBS) was purchased from Tocris Bioscience Inc. (Minneapolis, MN, USA). T98G human brain cancer cells were purchased from RIKEN BRC CELL BANK (RIKEN BRC) (Ibaraki, Japan).

2.2. Fabrication and Characterisation of Nanofibre Meshes

The PCL nanofibre meshes were fabricated according to our previously published procedure.[25,26] Briefly, electrospinning solutions were prepared by dissolving PCL in HFIP at concentrations of 2.8, 4.2 and 8.0% (w/w$_{(HFIP)}$) (Mw= 80k) or 8.4 (w/w$_{(HFIP)}$) (Mw= 45k), respectively. The MNPs and TMZ were dissolved in the PCL solution at concentrations of 10-30% and 10% (w/w$_{(PCL)}$), respectively. The nonwoven nanofibre meshes were produced through an electrospinning system (Nanon-01A, MECC Co., Ltd., Fukuoka, Japan). A positive voltage of 25 kV was applied to the polymer solution to overcome the liquid surface tension and enable the formation of a polymer jet. The nanofibres were collected on a collector plate 15 cm from the syringe needle. The flow rate was set at 1.0 mL/h, and the experiment was performed at room temperature. The morphology of the nanofibres was observed by scanning electron microscopy (SEM (S-4800), Hitachi High-Technologies Corporation, Tokyo, Japan, field emission scanning electron microscopy (FE-SEM) (S-8000) + energy dispersive X-ray spectroscopy (EDX), Hitachi High-Technologies Corporation, Tokyo, Japan) using secondary electrons after platinum (Pt) coating the surface of the nanofibres. The diameter of the nanofibres was determined using image analysis software (Image J). The chemical characteristic of the prepared nanofiber meshes were processed by the Fourier transform infrared spectroscopy (FT-IR, IRAffinity-1S, Shimadzu Corporation, Kyoto, Japan) (4000~400 cm $^{-1}$). The loaded amounts of MNPs within the nanofibre meshes were determined by thermogravimetric analysis (TGA) in a temperature range of 25 to 600°C at 10°C/min (TG/DTA6200, Hitachi High-

Technologies Corporation, Tokyo, Japan,). The thermal properties of the PCL nanofibre meshes were characterised using differential scanning calorimetry (DSC) (7000X, Hitachi High-Technologies Corporation, Tokyo, Japan,). All samples were heated to 200°C and cooled to 0°C. The DSC curves were obtained at a rate of 10°C/min.

2.3. Heating Profiles for Nanofibre Meshes

The heat generation behaviour of the nanofibre meshes was explored by AMF irradiation. Nanofibre meshes were placed in a customised copper coil that generated AMF (480 A, amplitude 281 kHz frequency) with HOTSHOT 2 (Alonics Co., Ltd., Tokyo, Japan). The temperature of the nanofibre meshes was measured at a predetermined time interval by a forward-looking infrared (FL-IR) thermal camera (CPA-E6, FLIR Systems Japan K.K., Tokyo, Japan). Infrared thermal images were obtained for the nanofibre meshes loaded with 12.0 mg of MNPs under AMF irradiation for 15 min. Additionally, the time-dependent temperature changes of the the MNP-PCL nanofibre meshes with different amounts of MNPs during AMF irradiation were analysed.

2.4. Drug Release Kinetics

The release behaviour of TMZ from the nanofibres was assessed in phosphate buffered saline (PBS) solution with or without AMF irradiation. Nanofibre meshes (0.3 mg TMZ and 30 mg meshes for each piece) were immersed in 5 mL of PBS solution by shaking (at 100 rpm) at 37°C for 28 d. The samples were exposed to AMF for 15 min every 3 d. At predetermined time intervals, 5 mL of PBS was withdrawn, and the same volume of fresh PBS was added. Subsequently, the absorbance (270 nm) of TMZ was measured using a Nanodrop (NanoDrop One C, Thermo Fisher Scientific, Wisconsin, USA). The accumulative releases of TMZ from the nanofibres were calculated according to their standard curves under PBS conditions. Known pharmacokinetic models, including zero order (Eq. (1)),[29] Higuchi (Eq. (2))[30] and Korsmeyer–Peppas (Eq. (3)) [31] were used to analyse the release mechanism of TMZ from PCL nanofibres. The kinetic parameters were obtained by nonlinear regression using MATLAB software (The MathWorks Inc., MA, USA).

$$Q = Q_0 - K_0 t \quad (1)$$

$$Q = K_H t^{1/2} \quad (2)$$

$$M_t/M_\infty = K_{KP} t^n \quad (3)$$

where Q_0 and Q are the initial TMZ content in nanofibres and TMZ released from nanofibres after time t, respectively. K_0, K_H and K_{KP} are the constant parameters of the zero-order, Higuchi and Korsmeyer–Peppas equations, respectively. When $n < 0.5$, Fickian diffusion-controlled release is implied, while $0.5 < n < 1.0$ indicates non-Fickian release and 1 stands for zero order (case II transport). When the n value exceeds 1.0, it indicates super case II transport.

2.5. Antitumour Efficacy

T98G (human brain cancer cell line) was cultured in RPMI supplemented with 10% (v/v) FBS and 1% penicillin-streptomycin under 5% CO_2 at 37°C. T98G cells were plated in a 96-well plate at 1.0×10^5 cells per well and incubated for 24 h. Thereafter, the medium was replaced with fresh culture medium heated to 37°C and supplemented with TMZ at the desired concentration. The cells were incubated for another 48 h. For the synergistic anticancer experiment, T98G cells were plated in a 35-mm plate at 10^6 cells per well for 24 h. Subsequently, a piece of nanofibre mesh (40 mg weight, 30% MNPs, 10% TMZ, 1×1 cm) was introduced to the 1 mL medium, which was exposed to AMF (480 A, amplitude 281 kHz frequency) for 15 min. The nanofibre mesh was immersed in the medium during treatment and removed by sterilized tweezer from each plate after 48h.The culture medium was then removed and incubated in a medium containing 10% (v/v) MTT assay reagent for 4 h at 37°C according to a protocol. Finally, the cell number was calculated according to the fluorescence intensity measured by a fluorescent plate reader (Infinite M Nano+, TECAN, Männedorf, Switzerland), and the average value was obtained from six measurements. Cell viability was expressed as a percentage of the control culture value. Untreated cells in the growth medium were used as controls.

2.6. Statistical Analysis

All experiments were performed three times, and the data are presented as means and standard deviations (SDs). Statistical analysis was conducted using Student's t-test. The difference between the results was statistically significant for $p < 0.05$ (*), $p < 0.01$ (**) and 0.001 (***).

3. Results and Discussion

3.1. Fabrication of Nanofibre Meshes

PCL is commonly used in biomedical applications as a biodegradable material and is approved by the U.S. Food and Drug Administration. Because of its biocompatibility, high hydrolytic activity and desirable processability, PCL is widely used for drug delivery and tissue engineering.[32] Electrospinning is a simple and versatile technique used to fabricate nanoscale-diameter nanofibres from various polymeric materials.[33,34] We have previously reported several PCL nanofibre meshes loaded with therapeutic agents such as anticancer drugs[24–26] and inactivated viruses.[35] In this study, we fabricated the TMZ and MNPs loaded PCL nanofibre meshes by electrospinning. All of sample were sterilized by ethylene oxide gas (EOG) after electrospinning.

Figure 1A(a–c) shows SEM images of various electrospun TMZ-loaded nanofibres of different diameters prepared by adjusting the concentration of PCL to 2.8, 4.2 and 8.0% (w/w) in HFIP. As shown in **Figure 2A**, the nanofibre diameters increased as the PCL concentration increased, and the average diameters of the various PCL-based nanofibres ranged from 280 nm to 1800 nm. It has been reported that the increase in the viscoelastic force against axial elongation during electrospinning injection can increase the fibre diameter.[36,37] From TGA measurement (**Figure S1B**), successful incorporation of MNPs were observed and the fibre diameters of MNPs-loaded nanofibre were almost constant (**Figure S1A,C**). **Figure 1A(d,e)** shows SEM images of

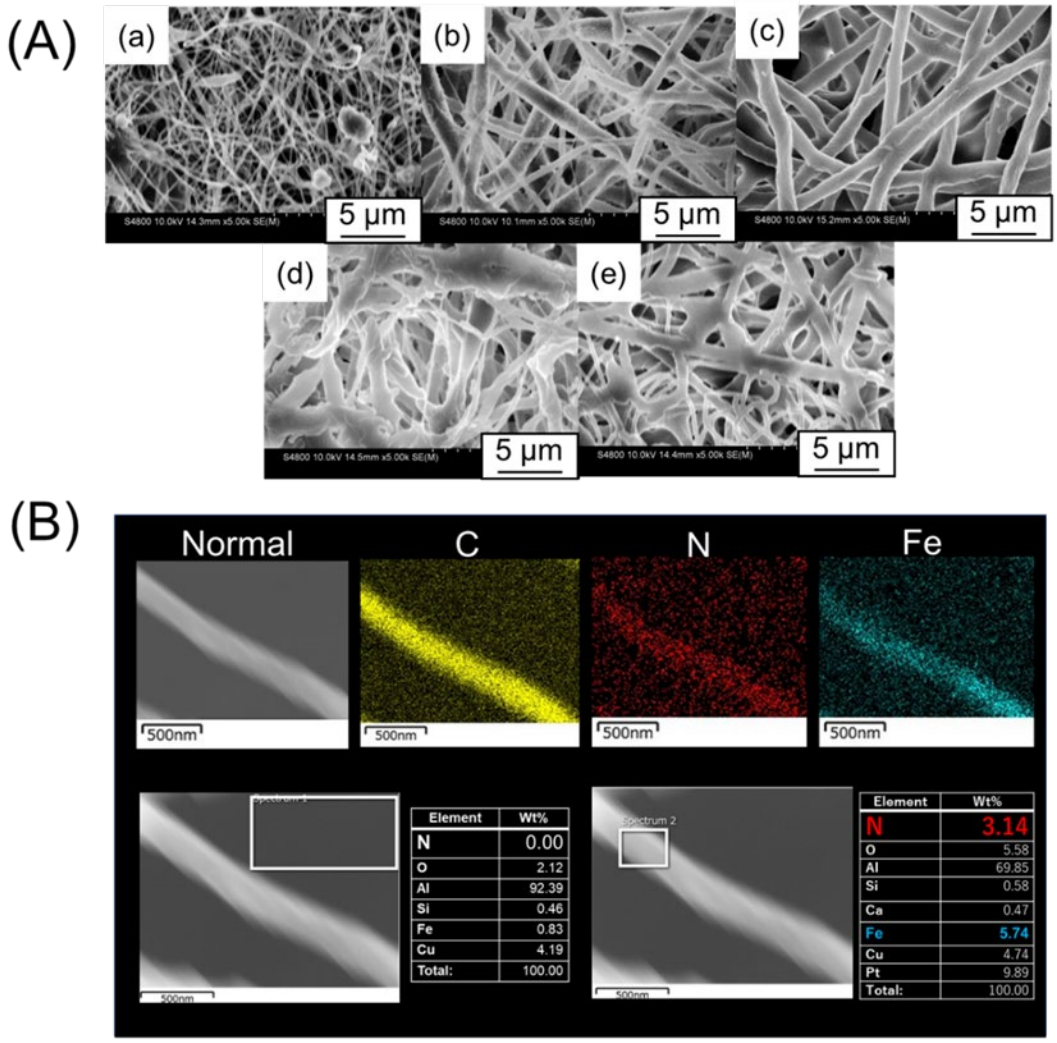

Figure 1. (A). SEM images of PCL-based nanofibre meshes with different concentrations (a: 2.3 wt%, b: 4.2 wt%, c: 8.0 wt% of PCL 80k) and molecular weights (d: 45k, e: mixed 45k–80k). **(B)**. SEM-EDX elemental mapping images of MNP/TMZ-PCL nanofibre. (FE-SEM (S-8000) + EDX, 10 kV, 10 eV).

nanofibre meshes fabricated from PCLs with different molecular weights. **Figure 1B** shows the energy-dispersive X-ray spectroscopy (EDX) mapping of MNP/TMZ-PCL nanofibres. These images show the homogeneous distribution of MNPs (iron (Fe) element) and TMZ (nitrogen (N) element) in the entire meshes and show that TMZ and MNPs are encapsulated in the nanofibres. **Figure 2B** summarises the average diameter of the nanofibres of PCL with different molecular weights ranged from 400 nm to 812 nm.

The ultimate tensile strength (UTS) of 80k-PCL nanofiber mesh was around 2.67 MPa, in the samples of thickness 0.5mm, and width 50 mm. This result indicates that the mechanical stability of our meshes is flexible and tough enough to be manipulated and implanted by surgical tools.

From the **Figure 3**, PCL-derived peaks C-O (2950 cm^{-1}) and C=O (1730 cm^{-1}) were observed in PCL nanofibre mesh. In addition, MNPs-derived peaks (Fe-O, 561 cm^{-1}) and TMZ-derived peaks (N-H, 3380, 3100 cm^{-1}) were also observed in the PCL-MNPs-TMZ mesh. Therefore, we consider that MNPs and

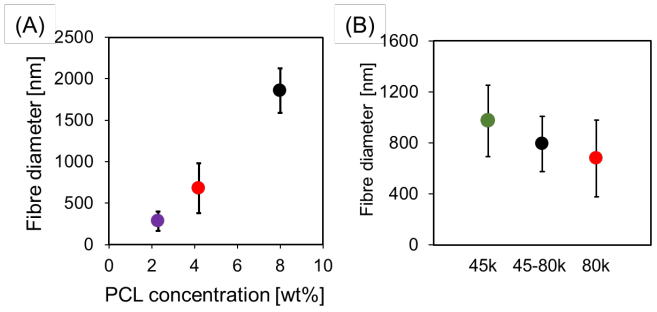

Figure 2. Average diameters of nanofibre mesh by (A) PCL concentration and (B) PCL molecular weight obtained using Image J.

TMZ were present in PCL nanofibres while maintaining their chemical structures.

3.2. TMZ Release Profiles and Kinetic Studies

Long-term release is difficult to achieve with nanoparticle-based CNS drugs because the penetration efficiency of most CNS drugs into the brain parenchyma is rather limited due to the existence of the BBB.[38] Compared to such nanoparticle-based

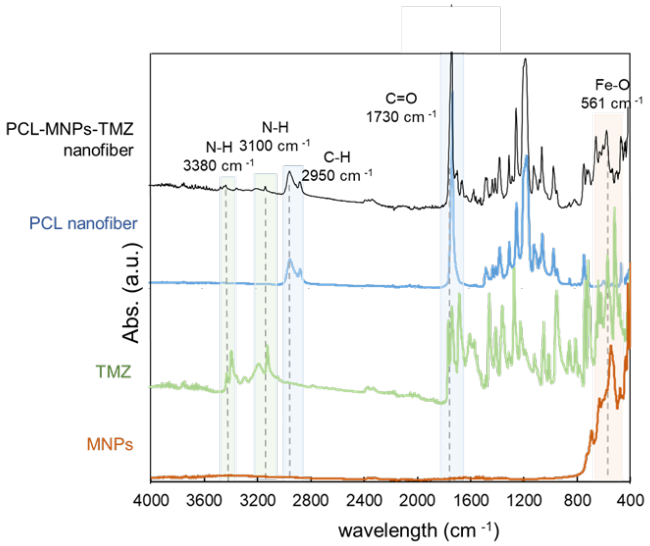

Figure 3. Chemical characteristics of the prepared nanofibers mesh by measuring FT-IR.

drug delivery platforms, nanofibre meshes are characterised by a high drug-loading capacity and long-term sustained localised release. Therefore, this study focused on the sustained release of TMZ from nanofibre meshes. As shown in **Figure 4A**, PCL 45k nanofibre meshes showed an initial burst release of TMZ. On the other hand, PCL 80k nanofibre meshes achieved the sustained release over 2 weeks. This is because the number of OH-terminal groups inside the nanofibre increases as the PCL molecular weight decreases, which makes the nanofibre more hydrophilic allowing rapid TMZ release. This result indicates that drug release rate can be controlled by the molecular weight of PCL without incorporating any other additives. The PCL 80k nanofibre was used for the following experiments.

As shown in **Figure 4B**, the release profiles of TMZ from nanofibre meshes with PCL of different fibre diameters showed that the TMZ release rate decreased as the fibre diameter increased. The results of fitted TMZ release data with kinetic models are summarised in **Table 1**. The Korsmeyer–Peppas model ($R^2 > 0.988$) best described the TMZ release data from 1800 nm PCL fibres (**Figure 5A**). In addition, the value of n increased with the nanofibre diameter, and TMZ was released following Fickian diffusion because $n < 0.5$. These results suggest that when the fibre diameter is small, the diffusion is the rate-limiting factor due to the increase in the specific surface area. In contrast, the rate-limiting factor is determined by the water molecules entering the nanofibre as the nanofibre diameter increases; thus, the TMZ release profile changes. The TMZ release data from the 1800 nm TMZ-loaded nanofibres showed good agreement with the Higuchi equation and reasonable

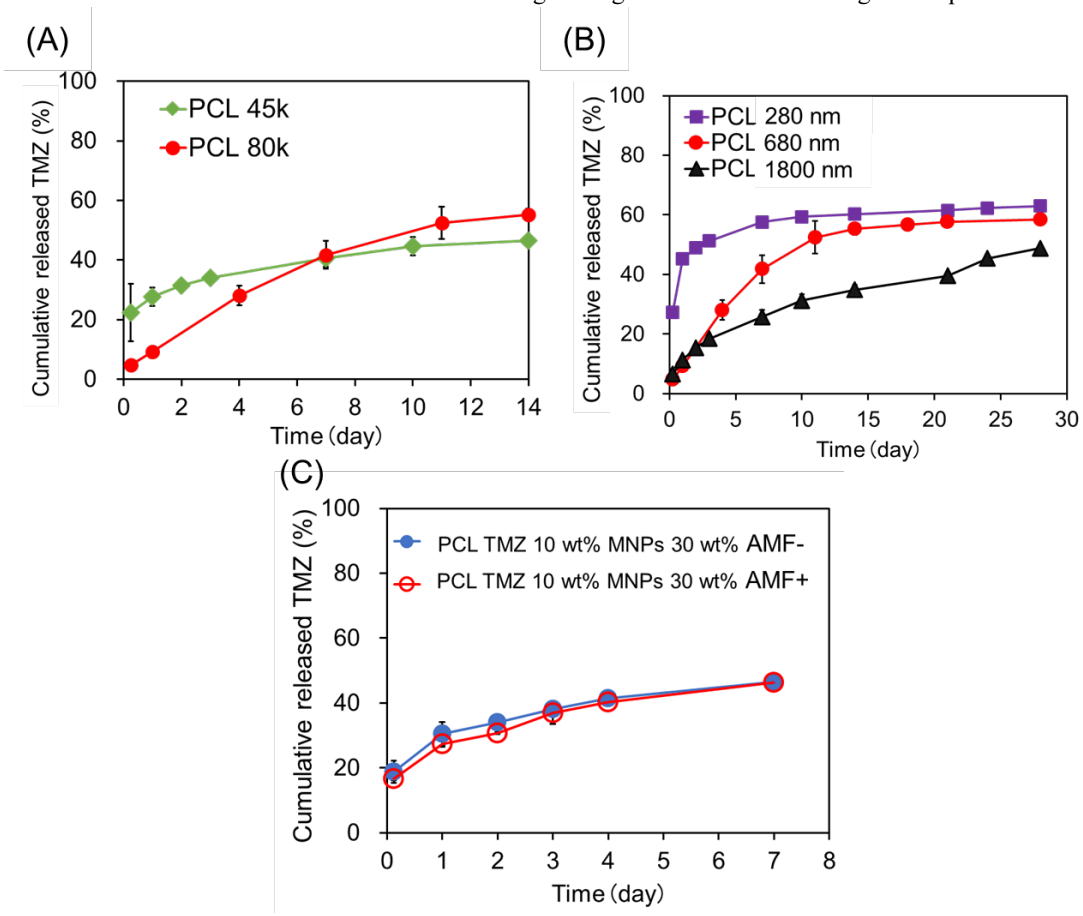

Figure 4. TMZ release profiles from PCL nanofibre meshes with (A) different PCL molecular weights (45k, 80k), (B) different nanofibre diameters and (C) with or without AMF application.

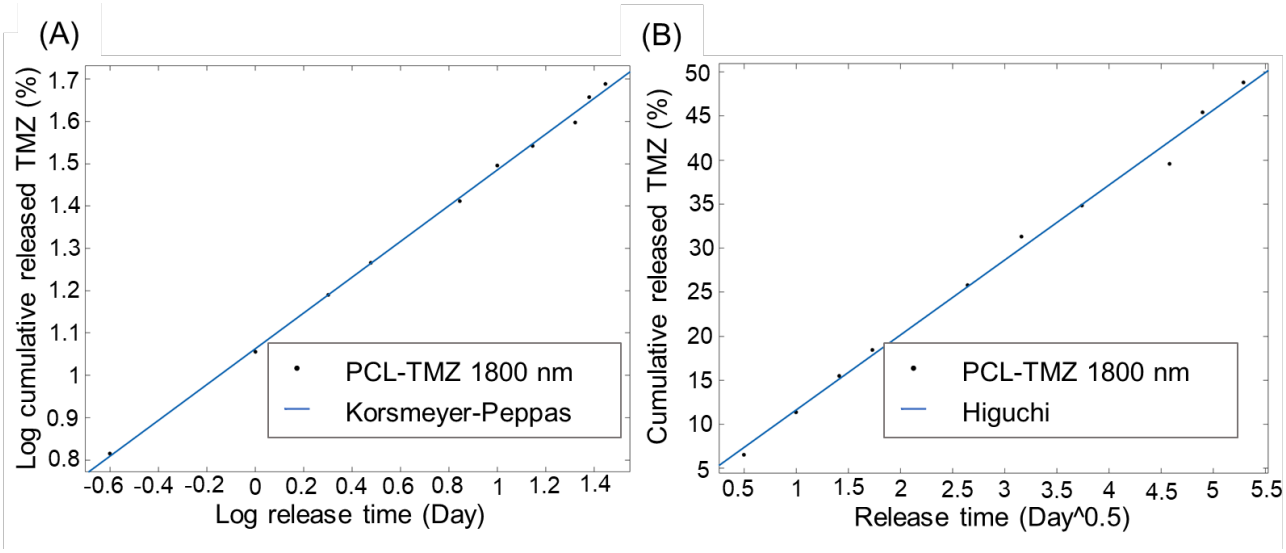

Figure 5. TMZ release profiles from 1800 nm PCL/TMZ nanofibres and fitting data with (A) Korsmeyer–Peppas kinetic model and (B) Higuchi equation.

Table 1.

Pharmacokinetic parameters for TMZ release from prepared nanofibres.

Formulation	Zero order		Higuchi		Korsmeyer–Peppas		
	K_0 (h^{-1})	R^2	K_H ($h^{-0.5}$)	R^2	n	K_{KP}	R^2
280 nm	0.8202	0.5756	15.44	-	0.1312	42.32	0.8996
680 nm	1.949	0.7547	13.17	0.9130	0.4129	16.78	0.9316
1800 nm	1.385	0.9447	9.325	**0.9827**	0.4300	11.35	**0.9950**

agreement with the zero-order equation (**Figure 5B**). These results indicate that the precise control of fibre diameter is important for the drug release profile from nanofibres. As shown in **Figure 4C**, MNP/TMZ-PCL nanofibres showed sustained release of TMZ. More than 30% of the content was released from MNP/TMZ-PCL in 7 d with or without AMF irradiation. It indicates that both MNPs and AMF irradiation did not affect the release of TMZ. Indeed, the melting temperature of PCL nanofibre meshes (59.6°C) is higher than the temperature increase by AMF application (42.6°C) as shown in **Figure S2**. Therefore, AMF application did not change the fibre morphology.

3.3. Heat Generation Behaviours of Nanofibre Meshes

Magnetic hyperthermia is a type of hyperthermia that uses the heat generated by MNPs when applying AMF to treat tumours.[27,28] The excellent tissue permeability of AMF makes it possible to respond precisely to tumours deep within organs. Therefore, it is important to measure the heating behaviours of MNPs in nanofibre meshes when AMF is applied. **Figure 6A** shows infrared thermal images of MNP-PCL nanofibre meshes with different MNP concentrations (10, 20 and 30 wt%) irradiated with AMF for 15 min. The temperature of the AMF-irradiated MNP-PCL (30 wt%) mesh increased from 27.2°C to 42.6°C. Furthermore, the time-dependent temperature changes of PCL and MNP-PCL nanofibre meshes during AMF irradiation were analysed. **Figure 6B** shows that the temperature of the nanofibre meshes reached equilibrium after a rapid increase

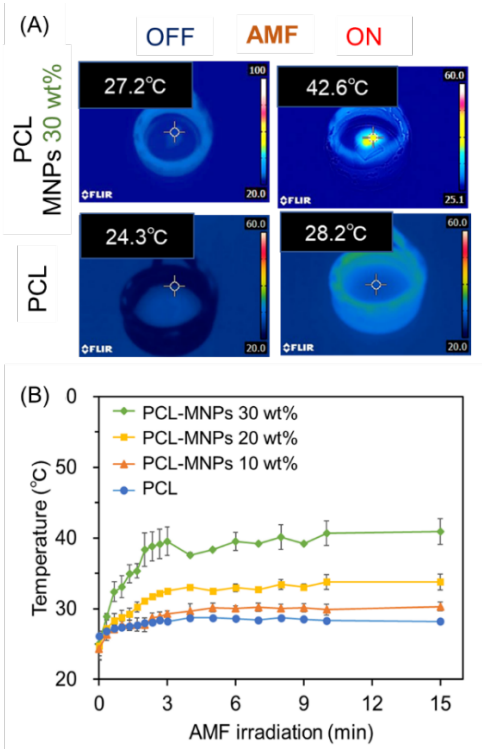

Figure 6. (A) Infrared thermal images of MNP-PCL nanofibre meshes with different MNPs concentrations during AMF application. (B) Heating profiles of MNP-PCL nanofibre meshes with different MNP concentrations during AMF irradiation at different times.

during the first 90 s of AMF irradiation. The temperature of the PCL mesh did not change significantly within 300 s. On the other hand, the temperature of the mesh loaded with 30 wt% MNPs increased to over 43°C in 300 s. Thus, the temperature of the MNP-loaded nanofibre meshes varied with concentration. Since the melting temperature of PCL nanofibre meshes is 59.6°C (**Figure S3**), their fibre morphology can be maintained at approximately 45°C. Therefore, we can apply AMF repeatedly to raise the temperature of the nanofibre meshes to treat localised hyperthermia. Although eddy currents caused by magnetic fields are known to have some effect on tissues and organ systems such as carbonisation and necrosis, we used only 281 kHz which is much lower than the safe frequency threshold for AMF (100–300 kHz).[40]

3.4. Anticancer Effects of Nanofibre Meshes

The viabilities of the T98G cells via TMZ concentrations are shown in **Figure S4**. The 50% inhibiting concentration (IC_{50}) of TMZ to T98G cells was determined to be 613 μg/mL. The different release profiles of TMZ depending on nanofibre diameter and PCL molecular weight were evaluated by T98G cell viability. As shown in **Figure S5**, cell viability decreased with increasing nanofibre diameter and with decreasing PCL molecular weight, consistent with the TMZ release amounts shown in **Figure 4A, B**.

It is known that the combination of chemotherapy and hyperthermia enhances the therapeutic effect because the anticancer drug is more easily taken up by cancer cells due to the heat. [27,28] Here, we evaluated the synergistic anticancer effect of hyperthermia using TMZ by the survival rate of T98G cells. As shown in **Figure 7**, the PCL nanofibre meshes without drugs as controls maintained nearly 100% cell viability, indicating that it is non-toxic to T98G cells. The TMZ-loaded nanofibre meshes and MNP-loaded nanofibre meshes each showed a 36% reduction in cell viability, indicating anticancer effects, while nanofibres loaded with both TMZ and MNPs showed a 76% reduction in cell viability and a higher anticancer effect compared to MNP-loaded nanofibre meshes and TMZ alone. Thus, MNP/TMZ nanofibre meshes killed more T98G cells compared to the control by the combined effect of TMZ and heating. Thus, these nanofibre meshes are expected to be an implantable therapeutic material that enables combined hyperthermia/chemotherapy to treat GBM.

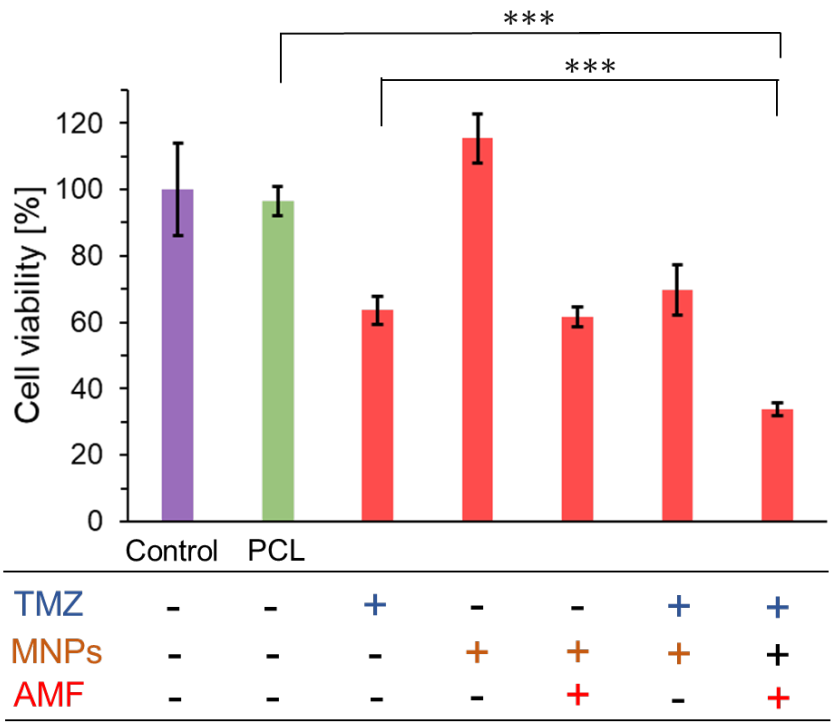

Figure 7. Viability of T98G cells treated with PCL-based nanofibre meshes under AMF irradiation. (Data are means ± SDs, n = 6, *** $p < 0.001$)

4. Conclusions

In this study, we fabricated novel PCL-based nanofibre meshes with MNPs and TMZ to achieve a combination therapy of hyperthermia and chemotherapy for the treatment of GBM. The nanofibre meshes were fabricated using an electrospinning method, and MNPs and TMZ were successfully incorporated in PCL nanofibres. The sustained release profiles of TMZ from the nanofibres for 4 weeks were favourable for the long-term maintenance of an effective drug concentration in the tumour site. We confirmed that the TMZ release profiles were successfully controlled by adjusting the fibre diameters, and the release rate of TMZ decreased with increasing the fibre diameter, achieving long-term sustained release. In *in vitro* experiments, the MNP/TMZ nanofibre meshes efficiently induced cell death through the synergistic anticancer effect arising from hyperthermia and TMZ chemotherapy. Given the lack of reports on brain tumour treatment materials containing the anticancer drug TMZ and MNPs in nanofibre meshes, we believe that this nanofibre mesh, which can be used in combination with chemotherapy and thermotherapy, fills this gap as a potential breakthrough treatment material that could replace the existing Gliadel® wafers.

Author Contributions

Emiho Oe https://orcid.org/0000-0001-7326-7740
Nanami Fujisawa http://orcid.org/0000-0002-8894-1790
Lili Chen http://orcid.org/0000-0001-8290-5230
Koichiro Uto http://orcid.org/0000-0001-7091-0585
Yoshitaka Matsumoto http://orcid.org/0000-0002-2074- 3042
Mitsuhiro Ebara http://orcid.org/0000-0002-7906-0350

Conflicts of interest

The authors declare no conflicts of interest.

Acknowledgements

This study was supported by the JSPS KAKENHI Grant-in-Aid for Scientific Research (B) [JP19H04476] and Grant-in-Aid for Transformative Research Areas (A) [JP20H05877]. The authors express their gratitude to the Nanotechnology Innovation Station for their support during the completion of this work.

References

1 A. Bernardi, E. Braganhol, E. Jager, F. Figueiro, M. I. Edelweiss, A. R. Pohlmann, S. S. Guterres and A. M. Battastini, *Cancer Lett.,* 2009, **281 (1)**, 53–63.
2 R. Stupp, M. E. Hegi, W. P. Mason, M. J. van den Bent, M. J. Taphoorn, R. C. Janzer, S. K. Ludwin, A. Allgeier, B. Fisher, K. Belanger, P. Hau, A. A. Brandes, J. Gijtenbeek, C. Marosi, C. J. Vecht, K. Mokhtari, P. Wesseling, S. Villa, E. Eisenhauer, T. Gorlia, M. Weller, D. Lacombe, J. G. Cairncross and R. O. Mirimanoff, *N. Engl. J. Med*, 2005, **352 (10)**, 577–581.
3 H. G. Welch, *JAMA*, 2000, **283(22)**, 2975–2978.
4 M. J. M. Darkes, G. L. Plosker and B. Jarvis, *AJCR*, 2002, **1**, 55–80.
5 S. M. Ward, M. Skinner, B. Saha and T. Emrick*, Mol. Pharmaceutics,* 2018, **15**, 5263–5276.
6 U. Akbar, T. Jones, J. Winestone, M. Michael, A. Shukla, Y. Sun and C. Duntsch, *J. NeuroOncol.,* 2009, **94 (2)**, 203–212.
7 E. M. Kemper, A. E. van Zandbergen, C. Cleypool, H. A. Mos, W. Boogerd, J. H. Beijnen and T. O. van Tellingen, *European Journal of Cancer,* 2004, **40**, 1269–1274.
8 M. Nagane, *Neurol. Med. Chir. (Tokyo),* 2015, **55**, 38–49.
9 P. P. Wang, J. Frazier and H. Brem, *Adv. Drug Deliv. Rev.*, 2002, **54 (7)**, 987–1013.
10 S. Vinchon-Petit, D. Jarnet, A. Paillard, J. P. Benoit, E. Garcion and P. Menei*, J. NeuroOncol.,* 2010, **97 (2)**, 195–205.
11 M. Westphal, D. C. Hilt, E. Bortey, P. Delavault, R. Olivares, P. C. Warnke, I. R. Whittle, J. Jääskeläinen and Z. Ram, *Neuro-Oncology*, 2003, **5(2)**, 79–88.
12 J. Perry, A. Chambers, K. Spithoff and N. Laperriere, *Current Oncology,* 2007, **14(5)**, 189–194.
13 S. Ni, X. Fan, J. Wang, H. Qi and X. Li, *Ann. Biomed. Eng.,* 2014, **42**, 214–221.
14 S. H. Ranganath and C. H. Wang, *Biomaterials*, 2008, **29**, 2996–3003.
15 A. Bazzazzadeha, B. Dizajia , N. Kianinejadb , A. Nouric and M. Irani*, Pharmaceutics*, 2020, **587**, 119674.
16 B. Ardeshirzadeh, N. Aboutalebi Anaraki, M. Irani, L. Roshanfekr Rad and S. Shamshiri*, Mater. Sci. Eng. C,* 2015, **48**, 384–390.
17 N. Aboutalebi Anaraki, L. Roshanfekr Rad, M. Irani and I. Haririan*, J. Appl. Polym. Sci.*, 2015, **132**, 1–9.
18 R. Salehi, M. Irani, M.-R. Rashidi, K. Nowruzi, M. Eskandani, I. Haririan and S. Davaran*, J. Polym. Mater.*, 2014, **63**, 609–619.
19 X. Xu, X. Chen, Z. Wang and X. Jing*, Eur. J. Pharm. Biopharm.,* 2009, **72**, 18–25.
20 S. Maretschek, A. Greiner and T. Kissel*, Journal of Controlled Release,* 2008, **127**, 180–187.
21 L. Moroni, R. Licht, J. de Boer, J. R. de Wijn and C. A. van Blitterswijk*, Biomaterials,* 2006, **27**, 4911–4922.
22 A. Zarghami, M. Irani, A. Mostafazadeh, M. Golpour, A. Heidarinasab and I. Haririan*, Fiber. Polym.*, 2015, **16**, 1201–1212.
23 S. Miyamura, T. Iwahashi, J. Sayanagi, Y. Hirai, K. Okada, K. Oka, E. Niiyama, K. Uto, M. Ebara, H. Yoshikawa, T. Murase and H. Tanaka, *PRS Global Open*, 2019.
24 T.Yoshida, M. Kaibori, N. Fujisawa, M. Ishizuka, F. Sumiyama, M. Hatta, H. Kosaka, K. Matsui, K. Suzuki, T. O. Akama, T. Katano, K. Yoshii, M. Ebara and M. Sekimoto, *Nanomaterials,* 2022, **12**, 1364.
25 E. Niiyama, K. Uto, C. Man Lee, K. Sakura and M. Ebara, *Adv. Healthc. Mater.,* 2019, **8**, 1900102.
26 L. Chen, N. Fujisawa, M. Takanohashi, M. Najmina, K. Uto and M. Ebara, *International Journal of Molecular Science*, 2021, **22**, 2542.
27 R. K. Singh, A. Srinivasan and G. P. Kothiyal, *J. Mater. Sci. Mater. Med.*, 2009, **147(20)**, 147–151.
28 E. J. Furlani and E. P. Furlani, *J. Magn. Magn. Mater*, 2007, **312**, 187–193.
29 D. S. T. Hsieh, W. D. Rhine and R. Langer, *Journal of Pharmaceutical Sciences*, 1983, **72(1)**, 17–23.
30 T. Higuchi, *J. Pharm. Sci.,* 1963, **52**, 1145–1149.
31 R. W. Korsmeyer, R. Gurny, E. Doelker, P. Buri and N. A. Peppas, *Int. J. Pharm.,* 1983, **15**, 25–35.
32 D. Rong, P. Chen, Y. Yang, Q. Li, W. Wan, X. Fang, J. Zhang, Z. Han, J. Tian and J. Ouyang, *J. Funct. Biomater.,* 2016, **7**, 6.
33 L. Azfarniam and M. Norouzi, *Fibers Polym.*, 2016, **17**, 298–304.
34 Y.-J. Kim, M. Ebara and T. Aoyagi, *Adv. Mater.*, 2016, **13**, 64203–64213.
35 T. Okada, E. Niiyama, K. Uto, T. Aoyagi and M. Ebara, *Materials*, 2016, **9**, 12.
36 R. M. Nezarati, M. B. Eifert and E. Cosgriff-Hernandez, *Tissue Engineering Part C: Methods*, 2013, **19**, 810–819.
37 R. Srikar, A. L. Yarin, C. M. Megaridis, A. V. Bazilevsky and E. Kelley, *Langmuir*, 2008, **24**, 965–974.
38 J. Xie, Z. Shenc, Y. Anraku, K. Kataoka and X. Chen, *Biomaterials,* 2019, **224**, 119491.
39 G. P. Skandalakis, D. R. Rivera, C. D. Rizea, A. Bouras, J. G. J. Raj, D. Bozec and C. G. Hadjipanayis, *International Journal of Hyperthermia,* 2020, **37(2)**, 3–19.
40 H. Mamiya, Y. Takeda, T. Naka, N. Kawazoe, G. Chen and B. Jeyadevan, *J. Nanomater.*, 2017, **20**, 1–7.

